Applied Thermal Engineering 258 (2025) 124515



Contents lists available at ScienceDirect

Applied Thermal Engineering

journal homepage: www.elsevier.com/locate/apthermeng



Research Paper



Development and tests of the novel configuration of the solar chimney with sensible heat storage

Krzysztof Sornek *, Rafał Figaj, Karolina Papis-Frączek

AGH University of Krakow, Faculty of Energy and Fuels, Department of Sustainable Energy Development, Krakow, Poland

ARTICLE INFO

Keywords:
Solar energy
Solar chimney
Passive solar energy
Solar air heater
Thermal storage
HVAC
Ventilation
Heat recovery

ABSTRACT

Heating, ventilation, and air conditioning systems account for a significant part of the energy usage in buildings and are primarily responsible for greenhouse gas emissions and operating costs. These can be lowered by the adoption of solar energy. This paper presents the developing and testing of a novel solar chimney with sensible heat storage. The thermal performance and potential contribution of the developed thermal chimney to decreasing residential buildings energy consumption in Polish climate conditions is investigated. The developed solar air chimney is composed of a novel accumulation material that allows for sensible heat storage. Solar radiation can heat the accumulation layer during the day and the stored energy can be used to preheat the ventilation air. The prototype of the solar chimney was tested in laboratory conditions using a dedicated experimental rig. Furthermore, numerical calculations were performed using TRNSYS software, where a validated dynamic numerical model was developed to simulate the performance of the device. The results show that airflow direction, volume, and the number of heated walls significantly impact the power transferred from the solar chimney walls to the air. The maximum power transferred from the solar chimney walls to the air per unit of surface varied from 360.2 W/m^2 (when all walls were heated) to 672.4 W/m^2 (when only one wall was heated). The validated model underestimates the outlet air temperature of the solar chimney by a maximum of 0.39 °C on average basis and shows that the increase of air temperature between −10 and 20 °C at 1000 W/m^2 determines a decrease of 12.5 % of the thermal output. The obtained results allow one to highlight that the proposed solution can be considered as a replacement for typical brick chimneys located on roofs or as a thermal storage wall.

1. Introduction

In the last decades, the energy consumed by buildings has increased rapidly, and now around 40 % of global energy consumption comes from the building sector [1]. Considering residential buildings, energy is consumed mainly by heating, ventilation, and air conditioning (HVAC) systems, domestic hot water installations (DHWs), kitchen equipment, and lighting [2,3]. To improve the energy performance of buildings and reduce their carbon footprint, it is crucial to introduce a net-zero energy building standard (NZEB). This standard can be achieved in different ways. The general outlines for developing NZEB buildings can be represented, for example, by a 5-step energy-saving strategy, which includes the following steps:

- Step 1: minimize as much as possible the heat consumption by buildings;
- Step 2: minimize as much as possible the electricity consumption by buildings;
- Step 3: use renewable energy sources for heat and electricity generation, including solar, wind and biomass energy;
- Step 4: regulate and monitor the energy consumption;
- Step 5: select the heat source fueled by a fuel as clean as possible.

Abbreviations: AF, Air Fan; *ASE*, Active Solar Energy; *AT*, Air Throttle; *CFD*, Computational Fluid Dynamics; *DHW*, Domestic Hot Water; *FTW*, Fluidized Trombe wall; *HVAC*, Heating, Ventilation, and Air Conditioning; *HS*, Heat Source; *NZEB*, Net-Zero Energy Building; *PC*, Computer; *PCM*, Phase Change Material; *PCMTW*, Trombe Wall with incorporated Phase Change Material; *PLC*, Programmable Logic Controller; *PSE*, Passive Solar Energy; *PV*, Photovoltaic; *PVTW*, Photovoltaic Trombe Wall; *RC*, Radiative Cooling; *SC*, Solar Chimney; *SCSHS*, Solar Chimney with Sensible Heat Storage; *TMW*, Trombe–Michel Wall; *TSW*, Thermal Storage Wall; *TW*, Trombe Wall; *WTW*, Water Trombe Wall; *ZTW*, Zigzag Trombe Wall.

* Corresponding author.
E-mail address: ksornek@agh.edu.pl (K. Sornek).

https://doi.org/10.1016/j.applthermaleng.2024.124515
Received 18 March 2024; Received in revised form 30 July 2024; Accepted 30 September 2024
Available online 1 October 2024
1359-4311/© 2024 The Author(s). Published by Elsevier Ltd. This is an open access article under the CC BY-NC-ND license (http://creativecommons.org/licenses/by-nc-nd/4.0/).

NZEBs are characterized by such features as the high thermal performance of the building envelope (including walls, roofs, windows, doors, etc.), the usage of clean energy (especially renewable energy sources), the limited usage of natural resources in an efficient way, and good indoor air quality. One of the most attractive options for using renewable energy sources in NZEBs is solar energy. Solar energy can be utilized in buildings in passive solar energy (PSE) and active solar energy (ASE) systems. Using conventional building elements to collect, store, and distribute solar energy (such as the roof and façade), PSE systems naturally use solar energy [4]. These systems fulfill the heating, cooling, and lighting needs, so they can be implemented in residential and non-residential buildings [5]. They can be realized in several ways, including the direct gain system, the thermal storage wall (TSW), the solar greenhouse, the roof pond, and the natural convective loop [6]. Among other options, combining the direct gain system, in which south-facing glass admits solar energy into the house, and solar TSWs can be considered a simple and efficient solution to improve the energy performance of buildings. The specific designs of TSWs depend on geographical latitudes and different climatic conditions. Worldwide literature includes the discussion of the following options: solar chimney integrated on the vertical wall (SC), Trombe wall (TW), Trombe wall with incorporated Phase Change Material (PCMTW), Photovoltaic Trombe Wall (PVTW), Trombe–Michel wall (TMW), Water Trombe wall (WTW), Zigzag Trombe wall (ZTW), and Fluidized Trombe wall (FTW) [7]. Furthermore, there are also available studies devoted to sensible heat storage materials, where evaluation of the optimal sensible heat storage material for maximizing solar still productivity is crucial [8].

The most commonly discussed solutions are SCs and TWs. SC is a technology that works on the buoyancy principle. This technology typically consists of a black hollow thermal mass with an opening at the top. When solar energy heats the chimney and the air within it, it produces an updraft flow of air in the chimney. The natural aspiration created at the chimney's base can ventilate the building. In the cooling mode, the air passes through the room and exits from the top of the chimney. In the heating mode, the air from the exterior is heated in the SC area and flows to the interior space [9]. SCs are considered a suitable solution for residential buildings due to their simplicity and zero maintenance costs [10]. Consequently, they contribute to an increase in efficiency for residential space heating and cooling in addition to a considerable reduction of greenhouse gas emissions. An idea of a solar chimney integrated on the vertical wall and operating in cooling and heating mode is shown in Fig. 1. Further common integrated configurations based on solar chimneys were considered and summarized in Ref. [11].

On the other hand, the classic TW is made of massive heat storage materials (for example, brick, concrete, or stone) and covered with glass [12]. The massive wall absorbs the solar energy transmitted through the glazing. Between these layers, the air gap determines an air flow by natural convection. The energy is transferred into the building by conduction (through the thermal wall) and convection (using heated air that flows upward due to the buoyancy effect) [13]. Heating the storage wall causes fluctuations in temperature on the inner surface during the day and the night. Filling the masonry walls with phase change material (PCM) can reduce these fluctuations. Furthermore, incorporating PCM with TW increases the possibility of obtaining thermal energy from solar radiation. PCM can store large amounts of heat during their phase transition (latent heat) without a significant increase in temperature [14]. An idea of classic TW and TW incorporated with PCM is shown in Fig. 2.

Various configurations of solar TSWs have been investigated in the literature. As a solar-assisted ventilation system, the SCs have been widely studied and applied in various types of buildings [15]. Shi et al. [16] summarized four groups of factors influencing SC performance, i.e., the configuration of the SC and building, installation methods, material properties, and the impact of the external environment. The authors concluded that changing the system's configuration is the most convenient and effective way of improving performance. Moreover, it was stated that the continuous development of new materials also affects the performance of SCs. Villar-Ramos et al. [17] presented the design, construction, and thermal evaluation of a single-channel SC with a

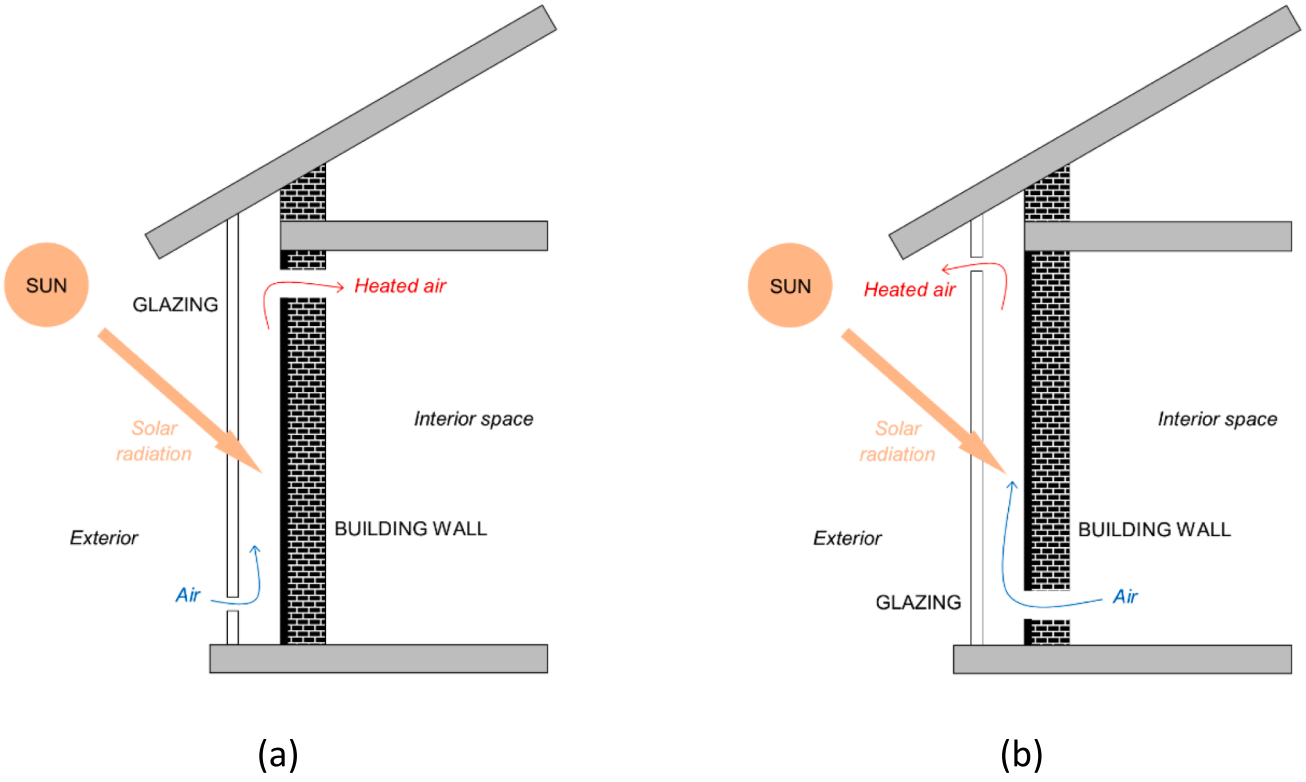


Fig. 1. The idea of a solar chimney integrated on the vertical wall in the heating mode (a) and cooling mode (b).

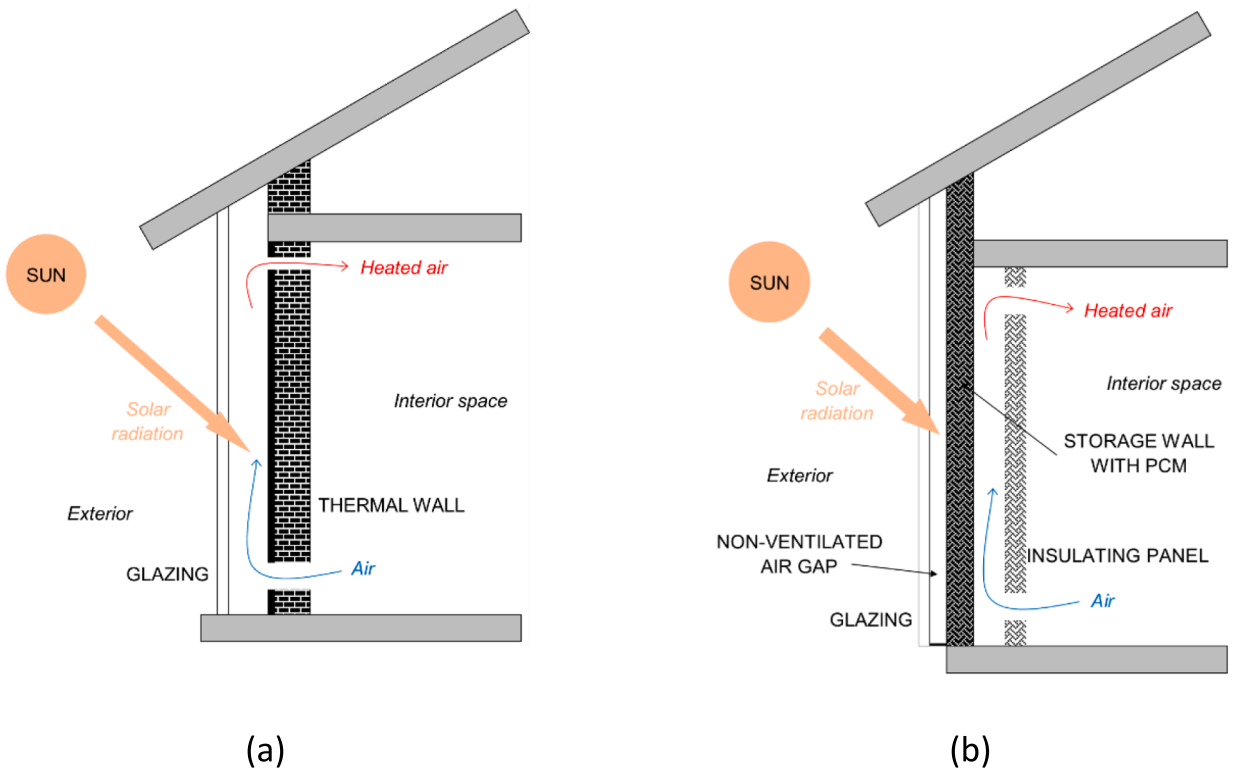


Fig. 2. The idea of a classic TW (a) and TW incorporated with PCM (b).

length of 2.0 m and a width of 0.8 m. A maximum temperature difference of 16.7 K was obtained during the tests. The authors concluded that an SC could be used as a passive ventilation system, where up to 5 times more airflow can be removed in an enclosure, with a maximum air change rate of 0.45 1/min and a maximum efficiency of almost 89.0 %. Zhang et al. [18] examined the airflow characteristics inside an SC, the attached ventilated multiple zones, and the SC performance under various configurations. By increasing the chimney height from 3.0 to 5.0 m, the ventilation capacity increased by about 90.0 %, while moving the air inlet upward got a 57.3 % improvement in the ventilation rate. Zha et al. [19] studied the performance of an SC in a real building in Eastern China. In an SCH of 6.2 m length, 2.8 m width, and 0.35 m air gap, an airflow rate from 70.6 to 1887.6 m^3/h has been achieved during the daytime. Sivalakshmi et al. [20] conducted an experimental ventilation analysis by integrating an SC in a room located in India. The performance of wall heat stacks was evaluated for different air channel widths, and the ventilation performance of the room with multiple openings was examined. The experimental results showed that flow rate and air velocity at the chimney outlet increase with an increase in air channel breadth between the absorber and glass in the wall chimney. Shaari et al. [21] presented the effect of converging duct on SCH using a computational fluid dynamics (CFD) model. The authors studied the effect of four configurations of bottom–top edge length ratio (1:1, 1:0.8, 1:0.75, 1:0.5). Results showed that the 1:0.5 ratio gives the highest outlet velocity. In contrast, the 1:1 ratio provides the highest number of air changes per hour. Nguyen and Wells [22] used CFD models to predict the ventilation rate and thermal efficiency of SCs with four types of adjacent walls, different chimney configurations, and the heat source location. Shi and Chen [23] numerically investigated a composite wall integrated with an SC and a wet porous layer for evaporative cooling without the consumption of electricity. In this case, airflow was driven by the buoyancy effect, and the water for evaporation on the surface was supplied by capillary forces in the wet porous layer. As was observed, more convection between the airflow and the surface of the porous layer under higher solar irradiation and more evaporation on the surface of the wet porous layer under lower relative humidity were beneficial for cooling. The 3.3 K or 2.1 K lower temperature of the inner surface of the analyzed wall than the ambient temperature occurred at about 12:30 on a sunny day. Nateghi and Jahangir [24] proposed combining radiative cooling (RC) with natural ventilation in the form of RC-enhanced roof SC ventilation. Three opening configurations were arranged, and CFD methods were employed to simulate the case studies. The results indicated that the radiative cooling cavity improves the ventilation and cooling performance of the natural ventilation system. Furthermore, the viability of solar chimneys in multi-storey atrium buildings was examined numerically and theoretically by Shi et al. [25]. The authors developed a theoretical model, which was experimentally validated to predict the natural ventilation rate of solar chimneys when it is applied to the atrium with multiple air inlets. It was noticed that the same theoretical model could be applied to the atrium buildings with odd and even stores, but the area coefficients were different. The obtained results confirmed the viability of solar chimneys in complex buildings. On the other hand, Long et al. [26] established a dynamic model of the solar chimney with an earth-air heat exchanger. The simulation results suggested that pipe diameter and length were more critical parameters affecting the system's airflow rate and indoor thermal environment, compared to chimney height and solar collector length. By the thermal inertia of the subsoil, the annual fluctuation of the air temperature at the buried pipe outlet was reduced to 12.8–26.5 °C. The indoor temperature was maintained by the system within the thermal comfort range for most of the time, with a decreased average indoor air temperature of 4.4 °C in summer and an increased one of 6.4 °C in winter. Another aspect, i.e., the interaction of room opening and air inlet on solar chimney performance, was analyzed under both natural ventilation and smoke exhaustion modes by Shi et al. [27]. The numerical results of nineteen scenarios were first validated by reduced-scale experiment tests. Another twenty-five numerical scenarios for full-scale solar chimney rooms with different heights of air inlet (0.1–2.3 m) and window (0.6–1.8 m) were analyzed. As was observed, the height of the window showed limited effect on the flow rate under natural ventilation mode,

but the obvious effect on both the flow rate at the air inlet and the total flow rate (both window and air inlet) under smoke exhaustion mode was observed.

The worldwide literature also includes many studies focused on the improvements in the classic TW design. Lohmann and Santos [28] evaluated the thermal behavior of the TW incorporated in a lightweight steel frame compartment located in Coimbra (Portugal). The authors studied two identical cubic modules exposed to natural weather conditions and provided a validated dynamic model of the analyzed system. According to the results, a TW device significantly improved the module's thermal behavior and reduced heat consumption. Zhu et al. [29] discussed an improved approach to the TW, in which an insulated panel was installed on the inner side, vents were installed at the top and bottom, and fans were installed in the upper vents for stable air circulation control. The study analyzed the thermal performance of this composite TW, for which the heat load was 27.3 % less compared to the classic TW and 32.1 % less compared to the case without the TW. Then, the authors optimized the ventilation efficiency, the proportion of the TW in the room, and the type of glazing. Owczarek [30] analyzed the heat transfer in a massive brick wall operating in natural conditions. The results showed a significant difference between winter and summer data. In the summer, the maximum temperature difference between the external and internal surfaces of the wall was measured as 20.0 K, and the heat input was 80 W/m^2. During the winter months, the maximum temperature difference was 10.0 K, and the solar heat flux was lower than the energy loss through the wall. Miasik and Krason [31] studied the operation of a mass collector-storage wall integrated into the southern facade of a light-construction building. During the summer period, the roller shutters allowed the heat flux to be reduced by approx. 77 % and therefore limited the building overheating. In the winter, the TW's energy consumption level was comparable to a traditional wall (gains from solar radiation compensated for the lack of thermal insulation). Kostikov et al. [32] calculated the solar radiation intensity on a TW surface in Harbin (China). The results showed that the proposed TW led to 61 % annual heat energy savings, whereas in the coldest month, these savings were 32 %. Fidaros et al. [33] provided a 2D steady-state CFD model of a basic wall and validated it by comparison with the results of an energy balance model. Then, ten different geometrical configurations were analyzed and compared. According to the results, the optimum width of the air gap varied between 5 and 8 cm.

Further improving the energy efficiency of the buildings is possible by installing the PCMs to TWs because they can shave the peak heating load during the day. Licholai et al. [34] determined the influence of glazing parameters on the thermal performance of the TSW containing a PCM. Three glazing with different heat transfer coefficients and total solar energy transmittance factors were used in the experimental tests. A noticeable influence of the type of glazing on the barrier operation was found. Liu and Li [35] experimentally studied the thermal performance of a solar chimney without and with PCM. Three different modes were developed when the inclusion of the PCM was realized (closed-fully charging mode, open-partly charging mode, and open-fully charging mode). The results showed that the implementation of PCM reduced the airflow during the charging period but increased it during the discharging period compared with the solar chimney without PCM. The mean airflow rate for open partly charging mode during the phase change period was lower than that for closed mode (0.036 kg/s compared to 0.041 kg/s). The results also showed that for open-fully charging mode, the PCM took almost 11 h to fully melt, and the melting time was 57 % longer than that for closed mode. Also, Huang et al. [36] experimentally studied the thermal performance of an SCH with and without PCM under different system inclination angles (30°, 45°, and 60°). results indicated that the effect of the inclination angle on the convective heat transfer inside the PCM cannot be ignored. An angle of 45° was found to be the optimal inclination, under which the solar chimney with and without the PCM reached a maximum air velocity of 0.37 and 0.4 m/s. Compared to the 60° case, the melting times of the PCM in the 45° and 30° cases were prolonged by 3.3 % and 13.3 %, respectively. In addition to the experimental studies, a numerical model was developed, and a simulation was carried out. Mabrouki et al. [37] discussed TSW's operation aspects in Morocco's semi-oceanic climate. The authors concluded that a 3 cm air gap, a 0.9 m sunshade, and RT 28 HC product with a melting temperature range around 27–29 °C as paraffin PCM were the best options to reduce the energy demand. The annual energy consumption for the reference single-room house decreased from 1 285.6 kWh to 733.2 kWh when vents were added to the PCM Trombe wall, which resulted in a savings of about 43 %. Leang et al. [38] demonstrated the impact of PCM on the thermal performance of the TSW. Three dynamic models were investigated: a house without a solar wall, a house with a concrete solar wall, and a house with a PCMTW. The results showed that TSWs allowed for minimizing the heating demand by about 20 % compared to the reference house. Rehman et al. [39] proposed a novel configuration of a TSW made of brick equipped with two layers of PCM. The authors provided a numerical simulation of the charging and discharging cycles of PCMs for two months: June and January. Results showed that the melting fraction for two layers of PCMs was 71 % and 2 % in June, whereas in January, it was 58 % and 100 %. Furthermore, Liang et al. [40] numerically examined a TSW with integrated PCM for a mild winter climate. Several semicircular fins filled with graphene nanoparticles were mounted on the TSW. The effect of TSW height, the distance between the glass wall and absorber plate, the number of fins, the presence or absence of PCM in fins, and flux quantity on average room temperature was investigated. The authors concluded that using PCM in the fins lowered the room temperature during the day, but stored energy could heat the room in the afternoon. In the studies related to charging and discharging PCMs, Ebrahimnataj et al. [41] mathematically modeled the energy charging mechanism to determine the impact of design modifications on the thermofluidic behavior of a PCM filled in a triplex tube containment geometry. Mohammed [42] examined the energy discharge of a PCM-based air heat exchanger using a metal foam inside the heat transfer fluid channel. It is also worth noting, that the implementation of PCM has attracted wide attention for thermal regulation in the field of PV panels, as the hybrid PVPCM technology can not only achieve higher photovoltaic conversion efficiency but also make it possible to extract thermal energy stored in PCMs for cascade utilization. For example, the incorporation of PCM into the building-integrated semi-transparent photovoltaic system is a promising technology for regulating the enhanced surface temperature of the photovoltaic (PV) system [43,44].

Despite the many advantages of introducing PCMs to TSWs, their use is expensive. Moreover, due to the poor thermal conductivity of PCMs, the operation of latent heat thermal energy storage is restricted by the limited heat exchange rate between PCMs and heat sources or sinks [45]. The gap in the existing literature consists of the lack of studies where innovative solutions/materials are used for the built of solar chimneys. This paper presents an innovative approach to developing and testing the solar chimney with sensible heat storage (SCSHS) composed of inexpensive ceramic modules typically used in accumulative wood-fired stoves in the form of a heat accumulation system [46,47]. Moreover, a numerical simulation model is developed and validated in order to estimate the thermal performance of the solar chimney as a function of different operation conditions. The advantages of the proposed heat accumulation system can be used to construct solar TSWs in energy-saving, passive, and nearly zero energy buildings. The idea of the SCSHS is presented in Fig. 3, which includes two possible configurations: the solar chimney with sensible heat storage integrated on the vertical wall (a) and located on the building's roof.

The proposed configurations of the SCSHS differ in some geometrical aspects, such as the number of ceramic modules installed, the arrangement of the ceramic modules, the organization of the airflow (including the direction of the airflow), the area of the modules heated by the sun, etc. However, the detailed configuration of the SCSHS (including the length and layout of the ceramic modules) needs to be calculated

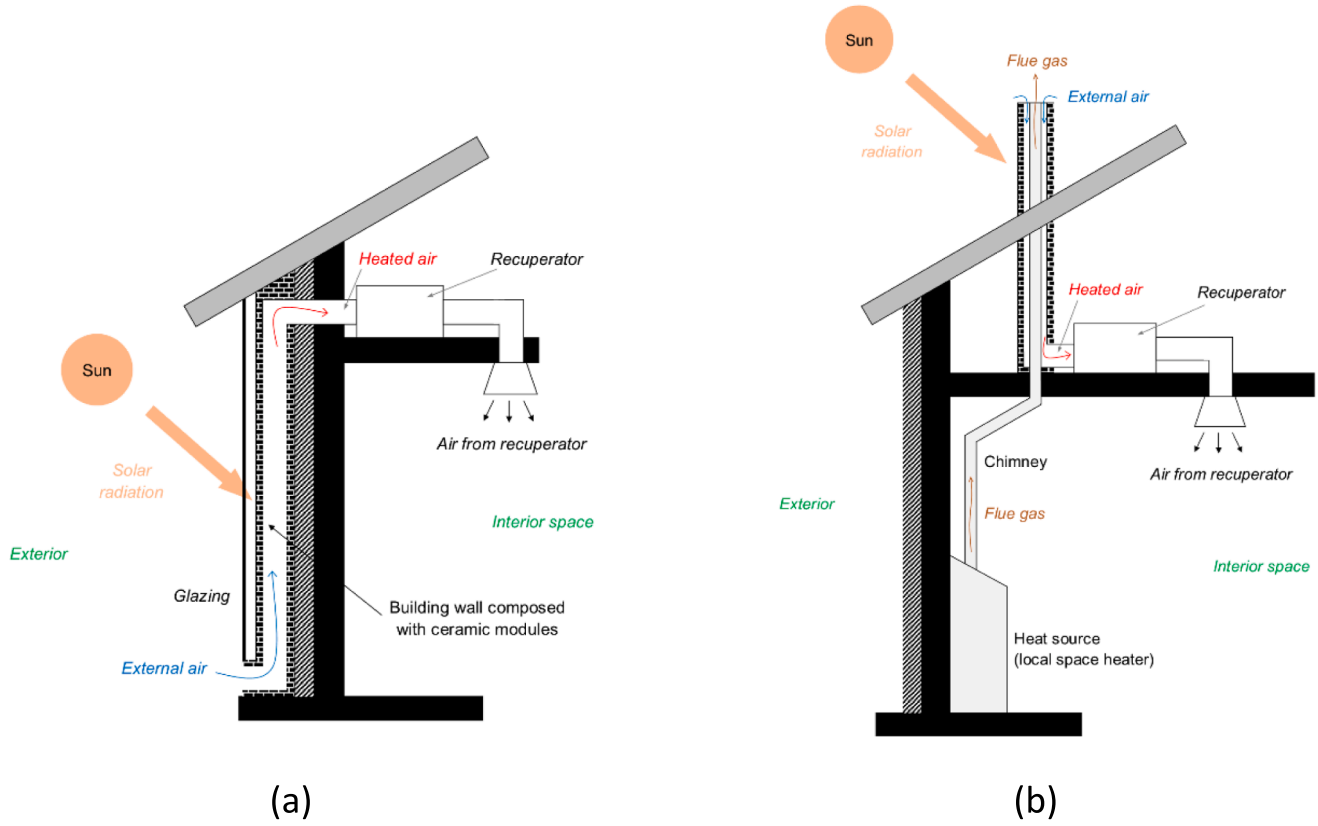


Fig. 3. The general idea of the solar chimney with sensible heat storage integrated on the vertical wall (a) and located on the building's roof (b).

according to the requirements of the individual building. In addition, it would be possible to optimize the airflow rate according to various factors, including real-time building occupancy, actual weather conditions (solar radiation, air temperature, wind, etc.), and expected daytime and night-time heat demand (via a dedicated AI-based controller).

The novelty and contribution of this work with respect to the existing literature is at least threefold:

- the construction of a modular solar chimney with sensible heat storage formed with ceramic modules was proposed for preheating ventilation air. The proposed solution allows for heat accumulation during the day and use at night when it is most needed;
- a special type of concrete characterized by high specific heat was used as sensible heat storage material as an alternative to phase change materials;
- a dedicated numerical model for the dynamic simulation of SCSHS was developed and validated, which can be used to investigate both the performance of SCSHS under different operation conditions and integration of SCSHS in buildings.

The findings presented in this paper put a basis to the adoption of solar chimneys adopting innovative ceramic/concrete materials in buildings in order to lower non-renewable energy sources dependency and operational costs.

2. Materials and methods

The presented investigations were divided into two following steps:

- discussion of the experimental studies conducted using a dedicated experimental rig,
- numerical simulations performed in TRNSYS software.

2.1. Experimental rig

The authors conducted measurements using an experimental rig located at the Faculty of Energy and Fuels, AGH University of Krakow. The essential part of the developed rig is the physical model of the solar chimney with sensible heat storage. SCSHS is made of a special type of concrete composed of ceramic aggregate with the content of iron and manganese oxides on the aluminum cement bond. At the current stage, the tested SCSHS is equipped with four ceramic modules with total dimensions of 0.25 x 0.25 x 1.0 m and an additional elbow used as a base. The accumulative ceramic modules are characterized by a thermal conductivity of 1.81 W/(m·K), a heat capacity of 640 J/(kg·K), and a 2 750 kg/m^3 density. They allow heat storage during the day and dissipate it after sunset. A general view of the single accumulative ceramic modules (in the form of straight channel, elbow, and tee) is shown in Fig. 4.

During the discussed experiments, the solar heat was simulated by a heat source (*HS*) equipped with 16 halogen lamps with individual electric power of 150 W. The halogen lamps are incandescent (temperature) light sources. They work by heating a tungsten filament to a temperature that emits light. The color temperature of halogen lamps is

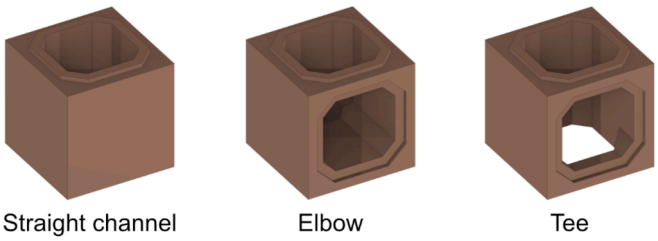


Fig. 4. A general view of the single accumulative ceramic modules in the form of straight channel, elbow, and tee.

higher than that of traditional incandescent lamps, so the maximum of the radiation spectrum is shifted towards shorter wavelengths (as a result, there is a small amount of ultraviolet radiation). On the other hand, halogen lamps emit infrared (heat) radiation in addition to visible radiation. The airflow is forced by an air fan (*AF*) and controlled by an air throttle (*AT*). Depending on the configuration, two airflow directions can be moved: from the bottom to the top and from the top to the bottom of the SCSHS. The main operation parameters are measured and recorded using a Programmable Logic Controller (PLC) and a dedicated application created in the CoDeSys software. The general scheme of the experimental rig is shown in Fig. 5 and Fig. 6, while the view of the rig is presented in Fig. 7.

The control and measurement system is equipped with the following elements:

- K-type (NiCR-Ni) thermocouple sensors with a measuring range of − 40 °C – 1200 °C and accuracy of ± 2.5 °C or ± 0.0075 × [t]) to measure air temperature at the inlet to the SCSHS and the outlet from the SCSHS (t_{air_in} and t_{air_out});
- thermoanemometer with a measuring range of 0 – 20 m/s and tolerance of ± 0.02 m/s + 3 % to measure airflow (V_{air});
- WAGO PFC200 PLC controller with a set of extension modules, including digital output modules and analogous input and output modules;
- the PC with CoDeSys software;

The tested SCSHS and the artificial heat source can be manually controlled by an operator or by using a specially developed control algorithm. Measured data is recorded in PC with a pre-set interval of 5 s.

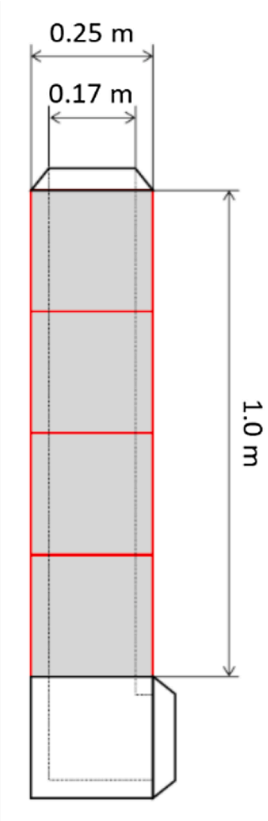


Fig. 6. Dimensions of the tested prototype of the SCSHS.

2.2. Experimental procedure

The experimental procedure was divided into four essential parts. In series 1 (selected as a basic scenario), the increase in air temperature and power transferred from the SCSHS walls to the ventilated air were determined when airflow volume was approximately 0.040 m3/s, airflow direction was set from top to bottom, and all SCSHS walls were heated by an artificial heat source. In series 2 and 3, different airflow volumes and directions were tested, while in series 4, different numbers of heated walls were examined. The initial airflow direction (i.e., from top to bottom) resulted from the fact that the proposed solution can replace a typical brick chimney located on the roof. However, considering various options for organizing airflow in SCSHS integrated with the vertical wall, airflow direction (from bottom to top) was also considered. The general description of each measurement series is given in Table 1.

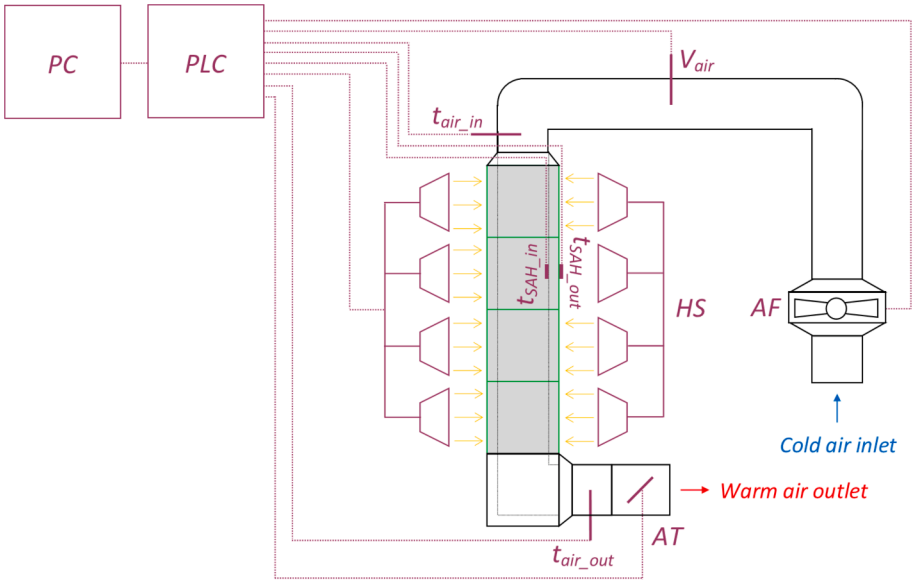


Fig. 5. Scheme of the experimental rig (*HS* – a heat source, *AF* – air fan, *AT* – air throttle, *PLC* – Programmable Logic Controller, *PC* – computer, t_{air_in} – the temperature at the inlet to the SCSHS, t_{air_out} – the temperature at the outlet from the SCSHS, V_{air} – airflow).

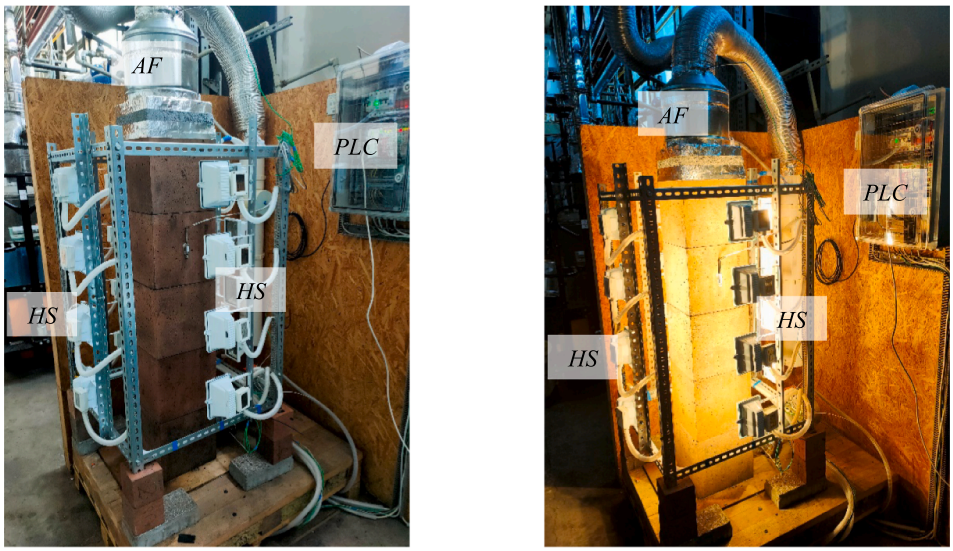


Fig. 7. The view of the experimental rig: when the artificial heat source is off (a), and when the artificial heat source is on (b) (*HS* – heat source, *AF* – air fan, *PLC* – programmable logic controller).

Table 1
Description of the measurement series carried out in the experimental investigations.

Measurement series	Airflow volume m^3/s	Airflow direction –	Number of heated walls –
Series 1 (basic)	0.040	top–bottom	4
Series 2A	0.028	top – bottom	4
Series 2B	0.054	top – bottom	4
Series 3	0.040	top – bottom	4
Series 4A	0.040	top – bottom	3
Series 4B	0.040	top – bottom	2
Series 4C	0.040	top – bottom	1

2.3. Numerical simulations in TRNSYS software

The numerical model of the developed SCSHS has been developed in TRNSYS simulation software [48], which is a tool dedicated to the dynamic simulation of energy components and systems. In particular, the model has been developed adopting a finite volume discretization method in which the thickness of the SCSHS was divided into equal parts. Each control volume consists of a layer of SCSHS material having a constant thickness equal to the total thickness of the single ceramic module divided by the number of adopted finite volumes, assumed to be four. Therefore, the discretization method divides SCSHS into frames shapes along the cross section of the chimney with a constant thickness and length of all the ceramic modules connected in a series. As regards the inner control volume, it has been assumed that it also contains the corners of the internal channels. Four control volumes were defined as follows:

- the first volume (1) consists of the external environment surrounding the external part of SCSHS and the first layer of SCSHS;
- the second (2) and third (3) volume consists of the internal layers of SCSHS;
- the fourth (4) volume consists of the inner layer and air flowing in the internal channel of SCSHS.

In particular, the second and third layers were adopted in order to simulate the temperature gradient within the block, and each adopted control volume comprised all four blocks of SCSHS. The structure of the control volume with the dimensions are reported in Fig. 8.

An unsteady state thermal balance equation has been used for each layer, taking into account gains and losses. Due to the fact that the model is based on simple/basic equations describing the heat transfer phenomena (convection, conduction and radiation), the formulas on the basis of the model has been here omitted for sake of brevity. To develop the model, the following assumptions have been adopted:

- uniform distribution of the radiation over the external surface of SCSHS;
- convective and radiative thermal losses from the external surface of SCSHS;
- radiative temperature of the external ambient equal to the temperature of the air surrounding SCSHS;
- convective losses the surface of the inner layer towards the air flowing within the internal channel (heating of the air passing through the internal channel);
- negligible radiative losses of the inner layer surface;
- conductive heat transfer between adjacent SCSHS layers;
- thermal properties of SCSHS material as reported in section 2.1;
- air heat capacity of 1006.4 J/(kg·K).

The boundary conditions for the four blocks were assumed as follows;

- the measured temperature of the air at the inlet of SCSHS was assumed as boundary condition for the external walls;
- the measured temperature of the air at the inlet of SCSHS was assumed as inlet temperature for the internal channel;
- the measured air flow rate was assumed for the inlet of the internal channel;
- the measured radiation intensity was assumed as boundary condition for the external walls.

The developed numerical model has been validated against experimental dynamic data regarding outlet air temperature. Moreover, a validated model has been used to determine the thermal performance of SCSHS as a function of the main operation parameters, such as radiation, inlet air temperature, and inlet air mass flow rate. The thermal

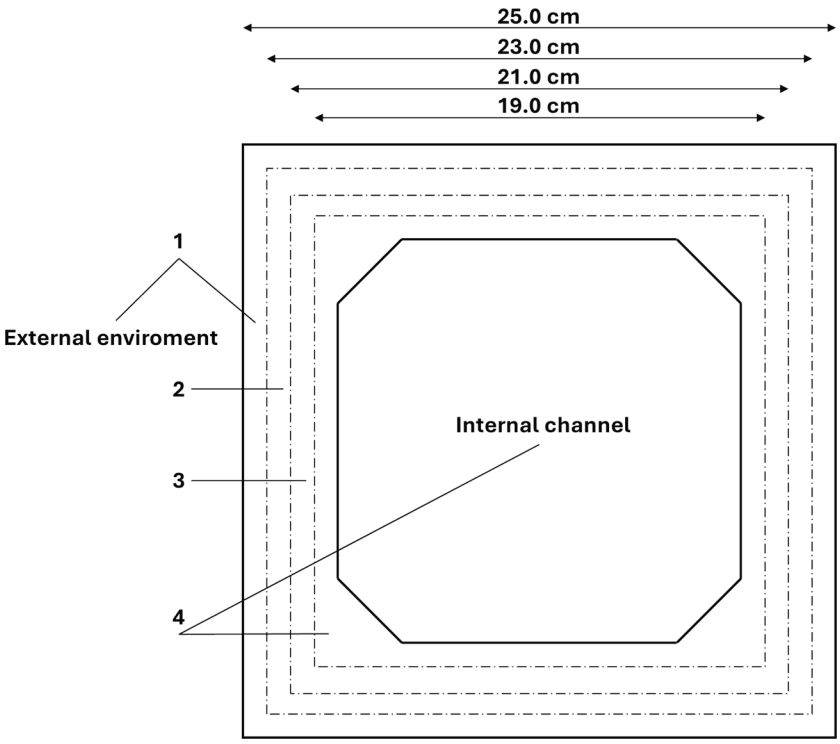


Fig. 8. Structure of the control volumes adopted in the numerical model.

performance has been determined, assuming that SCSHS achieves a stationary condition in terms of operation condition. The modelling and simulation process adopted in the study has been shown in Fig. 9.

3. Results and discussion

3.1. Analysis of the operational parameters of the SCSHS in the basic scenario

The basic scenario included the following assumptions: all four walls of the tested solar chimney with sensible heat storage were heating, the airflow direction was from the top to the bottom, and the airflow level was set to 0.040 m^3/s (series 1). Considering such operating conditions, the maximum observed increase of air temperature was approximately 7.2 ± 0.5 K (when stable temperature levels occurred). The maximum power transferred from the SCSHS walls to the air was consequently at a level of approximately 371.9 ± 32.8 W. Analyzing the time when the artificial heat source was active, the average value of temperature increase was 5.6 K, while the average power transferred to the air was 281.1 ± 29.1 W. On the other hand, these values were lower in the second part of the experiment, when the artificial heat source was turned off. Furthermore, the rate of temperature increase was calculated as about 2.0 K/h in time between the beginning of the experiment and minute 220 and 2.3 K/h in time between minutes 250 and 400. The higher drop in temperature of the SAH walls is connected with the lack of a heat source operation – no additional heat was supplied to the construction. These results show that the proposed construction of the SCSHS allows for both accumulating heat in the accumulation materials and preheating ventilation air simultaneously, as well as using the accumulated heat after sunset. Even though the efficiency of the proposed solution is higher during the Sun operation (here simulated by halogen lamps), a significant amount of accumulated heat can still be released when external heat flux does not occur. Furthermore, the proposed solution can minimize the heat transferred to the ventilation air during the day and avoid overheating internal spaces when direct heat gain occurs. The increase in air temperature and variations in power transferred from the SCSHS walls to air during series 1 are shown in Fig. 10.

3.2. The impact of airflow level and direction on the increase in air temperature

The airflow level and direction were selected as important parameters affecting the efficiency of the developed solar chimney with sensible heat storage. Starting from the airflow level, in real conditions, it results from the operating conditions of buildings and can vary over time (it can be higher during building occupation and lower when the building is vacant). Consequently, various airflow levels should be analyzed when the airflow direction is realized from the top to the bottom. In this work, two additional airflows were considered (0.028 m^3/s in series 2A and 0.054 m^3/s in series 2B) and compared with the basic scenario (0.040 m^3/s). As can be observed in Fig. 11a, the highest increase in air

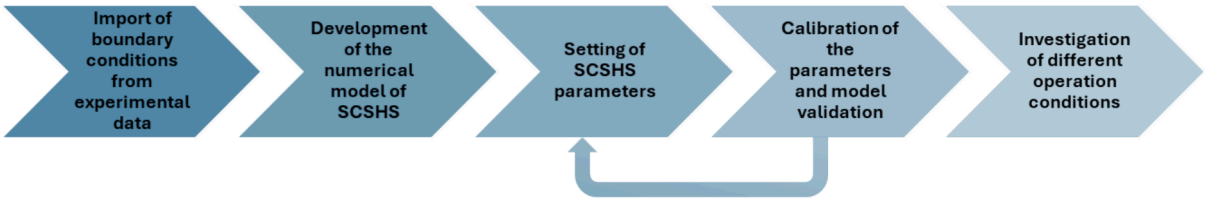


Fig. 9. Modelling and simulation process developed in TRNSYS software.

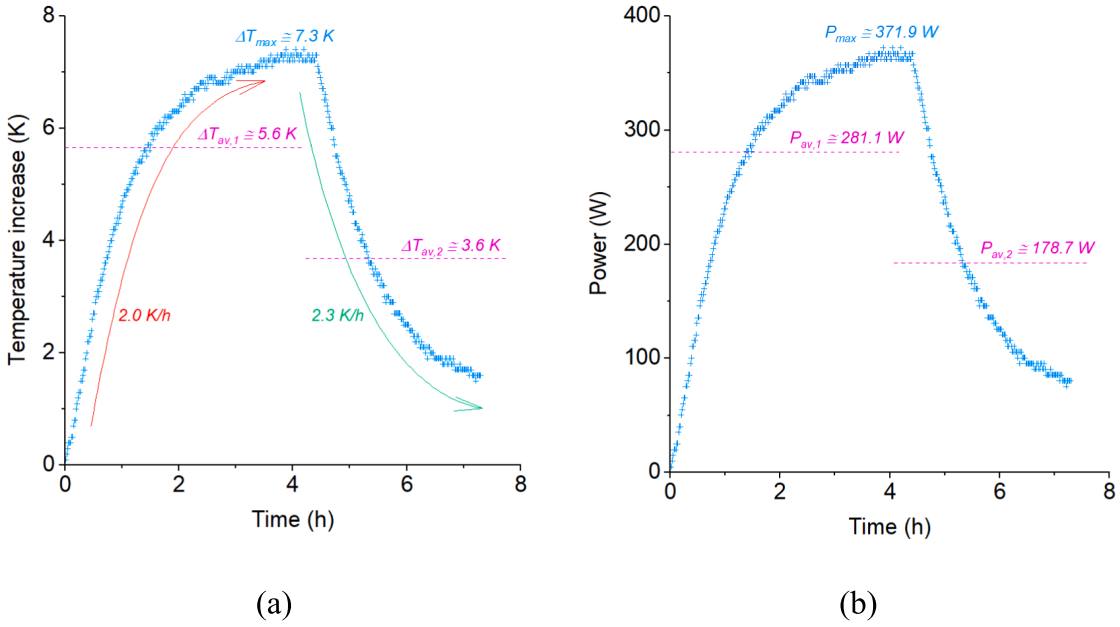


Fig. 10. The variations in a temperature increase (a) and power transferred from the SCSHS walls to air (b) during series 1.

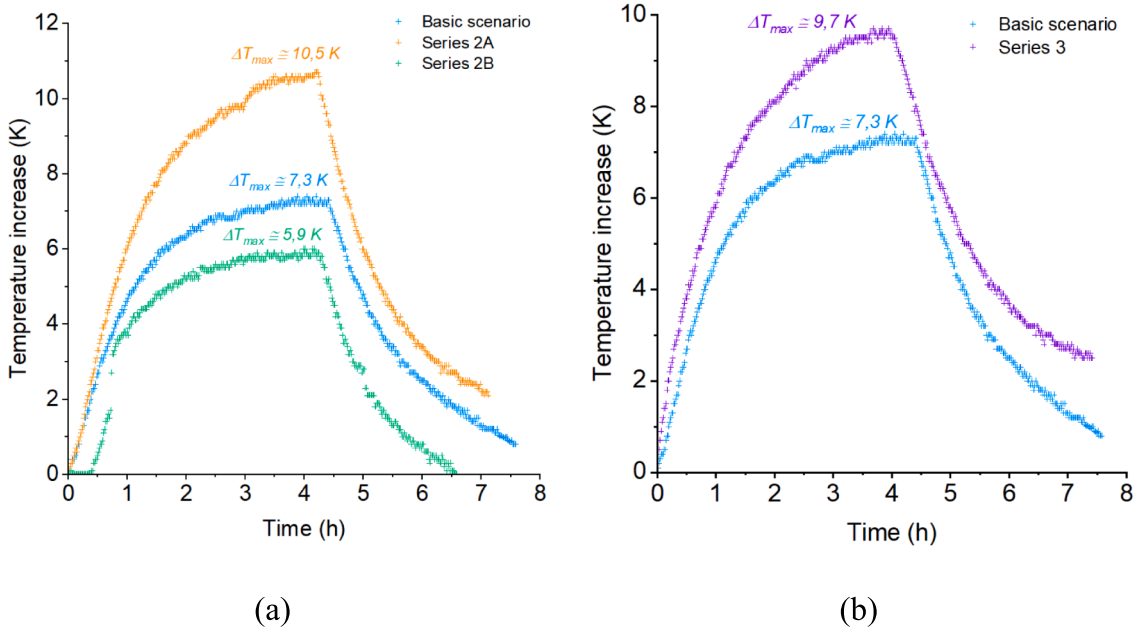


Fig. 11. The variations in temperature increase during series 2 (a) and series 3 (b).

temperature was 10.5 K in series 2A (higher by 3.2 K compared to the basic scenario), while the lowest increase in air temperature was 5.9 K in series 2B (lower by 2.4 K lower compared to the basic scenario). It is visible that the lower the flow, the more significant the temperature increase. The airflow direction can also significantly affect the temperature increase. Considering the time when stable temperature levels were observed, the average difference in air temperature at the inlet and outlet from the SCSHS was higher by 2.5 when air passed from the bottom to the top (series 3) compared to the situation when the air passed from the top to the bottom (basic scenario (see Fig. 11b).

In contrast to trends observed when temperature increase was analyzed during series 2A and 2B (when various airflows were compared), the highest power transferred from the SCSHS walls to the air was noted in series 2B. This maximum power was then at a level of 388.4 W. In series 2A, the power was 360.2 W, and in the basic scenario, it was 371.9 W. It can be concluded that the airflow impacts the increase in air temperature – the difference between values observed in the analyzed series and the basic scenario is approximately 3.2 to 4.4 % (on the other hand, differences in air temperature increase were much higher). On the other hand, considering the situation, when the air was passing from the bottom to the top, the maximum power transferred to the ventilation air under stable working conditions was approx. 484.4 W. It can be concluded that airflow direction essentially impacted heat transfer efficiency more than airflow volume. When air passes through the SCSHS from the bottom to the top, the efficiency can be higher by approximately 30.3 % compared to air passing through the SCSHS from top to bottom. The variations in power transferred from the SCSHS walls to the air are shown in Fig. 12.

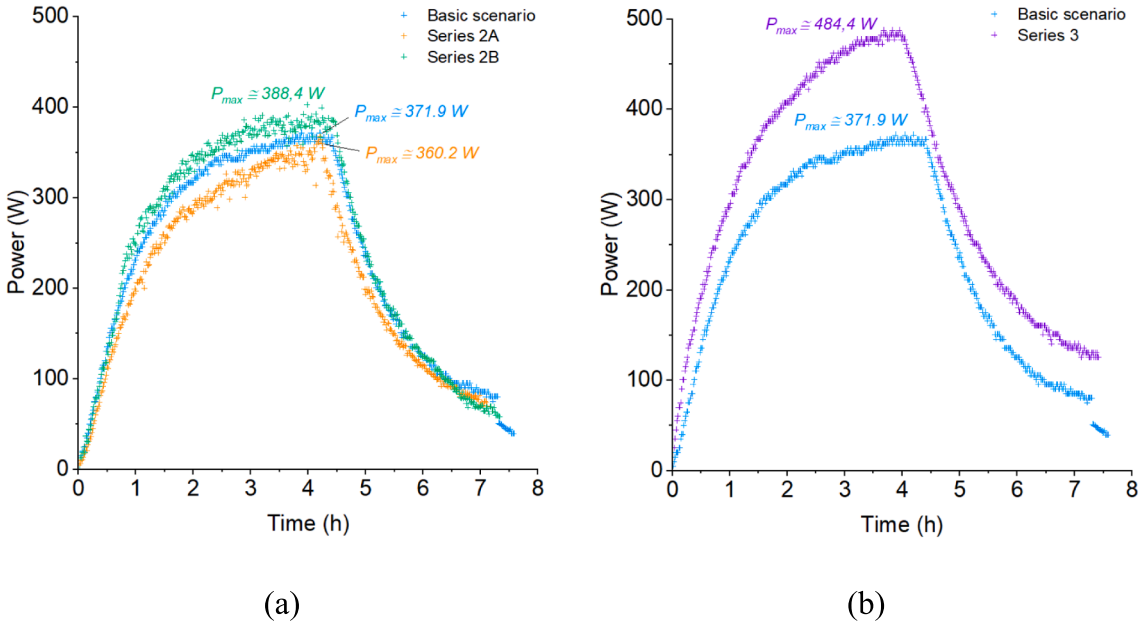


Fig. 12. The variations in power transferred from the SCSHS walls to air during series 2 (a) and series 3 (b).

3.3. The impact of the number of heated walls on the performance of the SAH

During the last experimental series, the impact of the number of simultaneously heated walls on the performance of the SCSHS was tested. The highest increase in air temperature was observed in the basic scenario when all four walls were heated – 7.3 K. When only part of the walls was heated, the increase in air temperature was lower and equal to 6.2 K, 4.6 K, and 3.3 K for three, two, and one heated walls, respectively. The last option occurs when the SCSHS operates as a solar chimney integrated with a vertical wall (series 4C). The increase in air temperature in series 4C is lower by 54.2 % compared to the basic scenario. Since chimneys have relatively low heights above the roof slope, the SCSHS integrated into the wall can be considered as a better option. The variations in temperature difference and power transferred from the SCSHS walls are presented in Fig. 13.

The obtained results are summarized in Table 2. It can be concluded that airflow direction, volume, and the number of heated walls significantly impact the power transferred from the developed solar chimney walls to the air. Also, considering the increase in air temperature, the above-mentioned factors are crucial. One difference can be observed when analyzing the impact of airflow on the operating parameters of the SCSHS. Higher airflow results in a lower temperature increase from one side but a higher amount of power transferred to the air from the second side. Energy transferred from the SCSHS walls to the air lowers the energy required to heat the rooms. In real conditions, the length of the SCSHS will be crucial from the standpoint of providing the required operating parameters of the air preheating system. As was calculated, the maximum power transferred from the SCSHS walls to the air per surface of 1 m^2 varied from 371.9 W/m^2 (when three walls were heated in series 4A) to 672.4 W/m^2 (when only one wall was heated in series 4C). This fact leads to the conclusion that the proposed solution can be

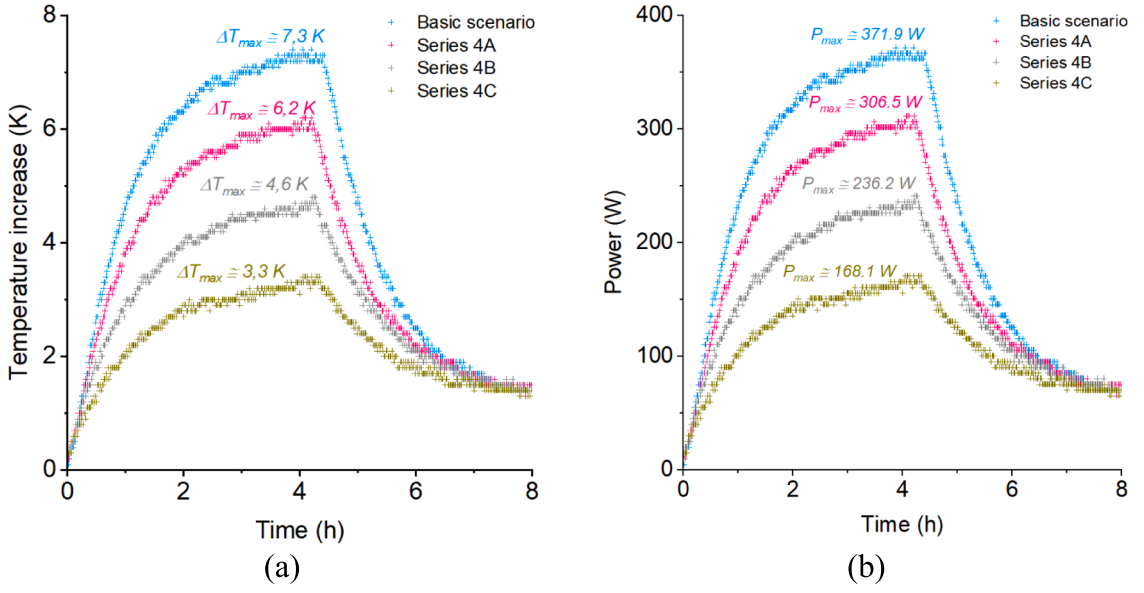


Fig. 13. The variations in a temperature difference (a) and power transferred from the SAH walls to air (b) during series 4.

Table 2
The summary of the results obtained in all measurement series in terms of maximum increase in air temperature, maximum thermal power and specific thermal power per unit of SCSHS area.

Series	The maximum increase in air temperature K	The maximum power transferred from the SCSHS walls to the air W	The maximum power transferred from the SCSHS walls to the air per surface W/m^2
Series 1 (basic)	7.3	371.9	371.9
Series 2A	10.5	360.2	360.2
Series 2B	5.9	388.4	388.4
Series 3	9.7	484.4	484.4
Series 4A	6.6	306.5	408.7
Series 4B	4.6	236.2	472.4
Series 4C	3.3	168.1	672.4

considered as a replacement for typical brick chimneys located on roofs or as a thermal storage wall.

3.4. Validation of the numerical model and numerical simulations

The developed dynamic simulation model has been validated using experimental data, such as inlet air mass flow rate, inlet air temperature, and outlet air temperature. In particular, the measurement series during which the air flow rate has been changed were used for validation. The validation was performed using the inlet air mass flow rate and temperature as inputs to the model and comparing the experimental outlet air temperature with the one calculated with the numerical model. The following parameters/inputs of the model have been calibrated to achieve the best fitting between experimental and numerical data: radiation intensity, external and internal surface convective heat exchange coefficient, radiation absorption, and emissivity coefficient of the external surface. The validation parameters and inputs were selected in order to minimize the integral of the absolute value of the difference between the experimental and numerical values of the outlet air temperatures. In order to find the best set of fitting parameters a design of experiments approach has been adopted, based on the repetition of simulations with different values of selected parameters. In the validation, in order to take into account the variation of the convective heat transfer coefficient as a function of the airflow rate, an empirical correlation has been developed that allows one to minimize the error between experimental and numerical data of the outlet air temperature.

The comparisons between experiments and simulations with validated model are reported in Fig. 14, Fig. 15, and Fig. 16 for the series 2A, 2B, and 2C, respectively. For all the simulations, according to the validation carried out, the radiation intensity, the convective heat transfer coefficient of the external surface, the radiation absorption, and the emissivity coefficient were set to 1 000 W/m^2, 2 $W/(m^2 \cdot K)$, 0.90 and 0.70, respectively. As concerns the internal convective heat transfer coefficient, it was found that the best fitting values are 8.0 $W/(m^2 \cdot K)$ for an airflow of 0.028 m^3/s (series 2A), 9.0 $W/(m^2 \cdot K)$ for an airflow of 0.040 m^3/s (series 2B) and 10.0 for an airflow of 0.054 m^3/s (series 2C).

It is worth noting that the developed model slightly underestimates the outlet air temperature of SCSHS once the radiation source is turned off. This occurs because the model does not take into account the surroundings of the SCSHS in the real installation. Indeed, the objects near the device have a certain thermal capacity and exchange heat with air in its proximity and with the device itself. In Table 3, minimum, maximum, and average absolute errors (experimental minus model data) have been reported for all series used in the validation.

Based on the results and taking into account a minimum error of ± 2.5 K in measuring air temperature, the developed model can be considered validated. It is worth noting that the model slightly underestimates the outlet air temperature on an average basis. Thus, it could be used to perform reliable simulations of energy systems and buildings integrating the SCSHS developed in this study. The validated model has been used to investigate the heat performance of SCSHS as a function of different operation conditions, such as radiation intensity, inlet air temperature, and inlet air mass flow rate. The simulations were carried out under stationary conditions and assumed constant values for

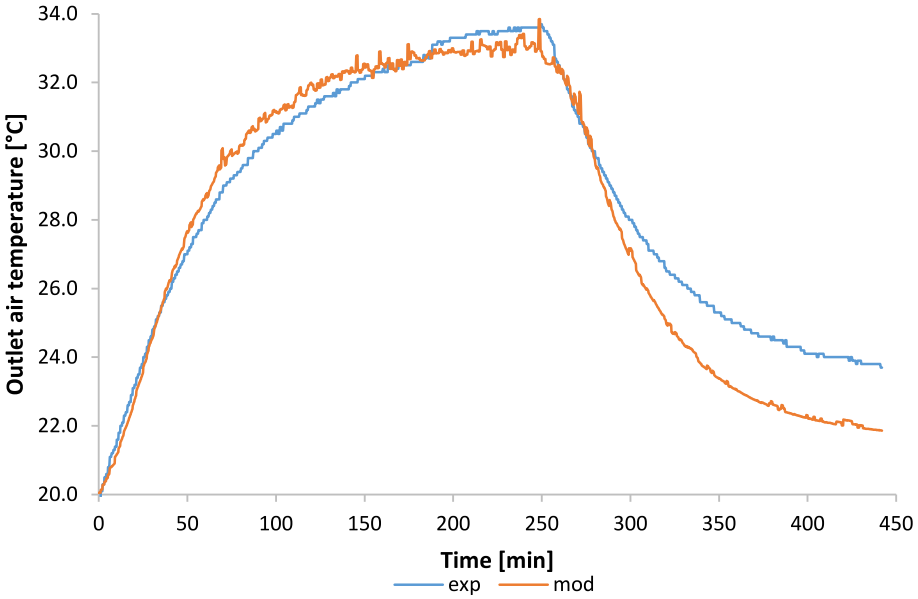


Fig. 14. Validation of the model in terms of outlet air temperature of series 2A, comparison between model and experimental data.

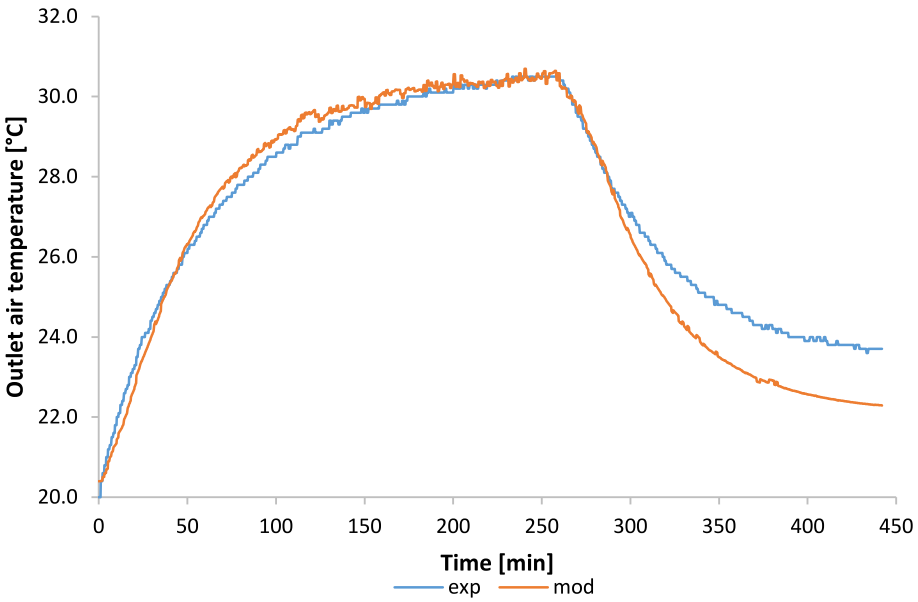


Fig. 15. Validation of the model in terms of outlet air temperature of series 2B, comparison between model and experimental data.

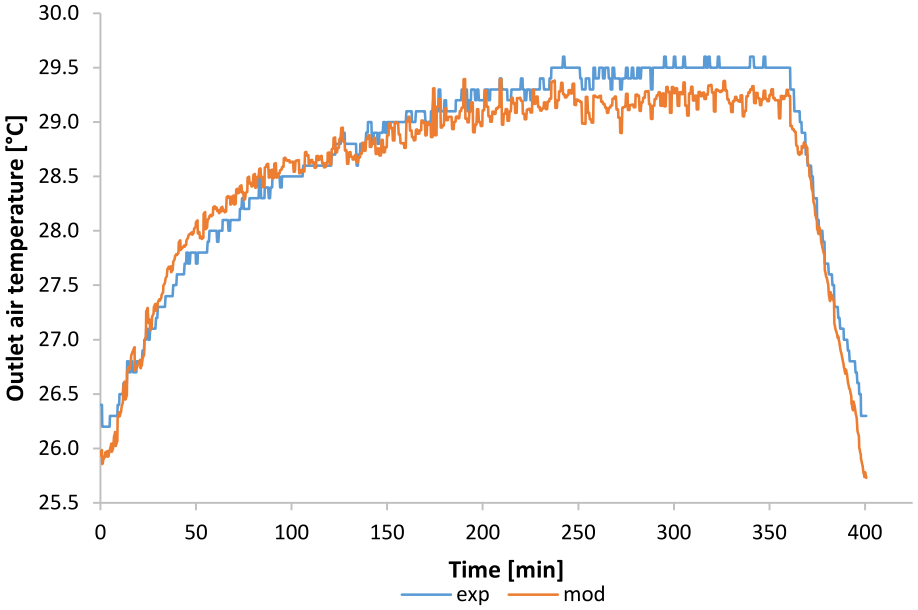


Fig. 16. Validation of the model in terms of outlet air temperature of series 2C, comparison between model and experimental data.

Table 3
Minimum, maximum, and average absolute errors (experimental minus model data) regarding the outlet air temperature.

Series	Error [K]		
	Minimum	Maximum	Average
Series 2A	−1.29	+2.10	+0.39
Series 2B	−0.59	+1.52	+0.33
Series 2C	−0.40	+0.57	+0.12

the operation conditions that were not varied in each analysis (1000 W/m^2 for radiation intensity, 10 °C for the inlet air temperature, and 200 kg/h for the air mass flow rate). In Fig. 17, the thermal power as a function of radiation intensity and inlet air temperature is shown. The results show that SCSHS thermal power is mainly affected by the radiation intensity and less by the inlet air temperature. This occurs because, basically, the thermal behavior of the device is governed by the heat exchange given by the source of radiation, similar to other solar energy collection technologies such as flat plate solar collectors. The heat transfer distribution is governed principally by the radiative heat source rather than the condition of the entering air. However, a higher effect of the air temperature on the thermal performance is achieved at higher radiation intensities. In fact, the increase of air temperature between −10 and 20 °C at 1000 W/m^2 determines a decrease of thermal power of 53.4 W, while for radiation of 100 W/m^2, the decrease is 8.9 W. Nevertheless, in percentage, the drop of power at 100 W/m^2 is higher (15.5 %) than the one achieved for 1000 W/m^2 (12.5 %) for the same temperature range.

In Fig. 18, the thermal power as a function of radiation intensity and inlet air temperature is shown. The analysis in this case reveals that the effect of a higher flow rate is more significant at higher radiation intensities. This occurs because the higher the radiation intensity, the

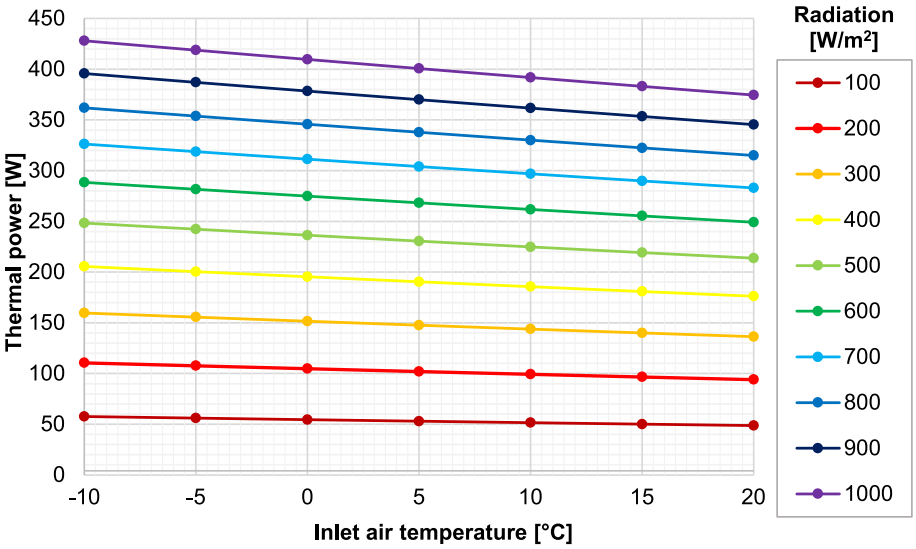


Fig. 17. Thermal power of SCSHS vs. radiation intensity vs. inlet air temperature.

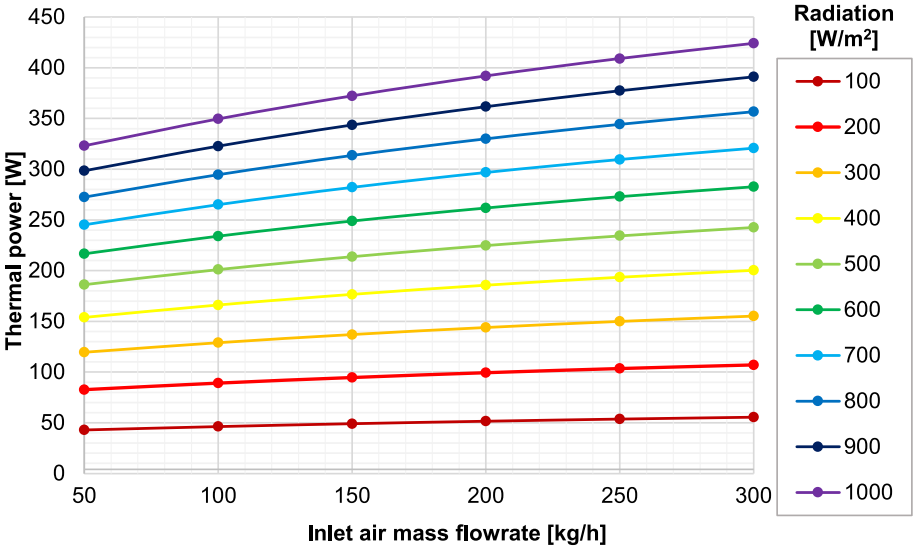


Fig. 18. Thermal power of SCSHS vs. radiation intensity vs. inlet air mass flow rate.

higher the temperature of the internal surface of SCSHS, thus increasing the airflow, the heat is extracted more efficiently. At 1 000 W/m^2, the thermal power increases by 100.9 W when the flow rate shifts from 50 kg/h to 300 kg/h, while for 100 W/m^2, the increase is 12.5 W.

Lastly, Fig. 19 shows the thermal power as a function of inlet air temperature and air mass flow rate. In this case, the relation between the thermal power and the inlet air temperature is practically linear at any flow rate at a fixed radiation intensity (1 000 W/m^2). The higher the inlet air temperature, the lower the temperature difference involved in the convection phenomenon, and the lower the thermal power of SCSHS. Moreover, it is interesting to note that the increase of the thermal power at a constant air temperature decreases when the air flow rate rises. This is achieved because the convective heat transfer is limited by the temperature regime inside SCSHS, which is mainly due to the radiation intensity and, in part, by the inlet air temperature.

4. Conclusions

This paper includes developing and testing a novel solar chimney with sensible heat storage. A novel concept of the device composed of accumulation material was proposed and investigated. In particular, the prototype was tested in laboratory conditions and numerical calculations were performed using TRNSYS software on the basis of a validated model simulating the dynamic behaviour of the device. The main conclusions of the paper are as follows:

- by using solar radiation (here, simulated by an artificial heat source), it is possible to heat the ceramic material and use the accumulated heat to preheat the ventilation air for the next hours (about 3);
- the power transferred from the solar chimney with sensible heat storage to the ventilation air depends mainly on radiation intensity, airflow direction and the number of heated walls;
- the maximum power transferred from the solar air heater walls to the air per unit of surface varies from 360.2 W/m^2 (when all walls are heated) to 672.4 W/m^2 (when only one wall is heated);
- the numerical model developed for the dynamic simulation of the solar chimney with sensible heat storage shows satisfactory agreement with the experimental data. Indeed, the model only slightly underestimates the outlet air temperature of 0.28 K on an average

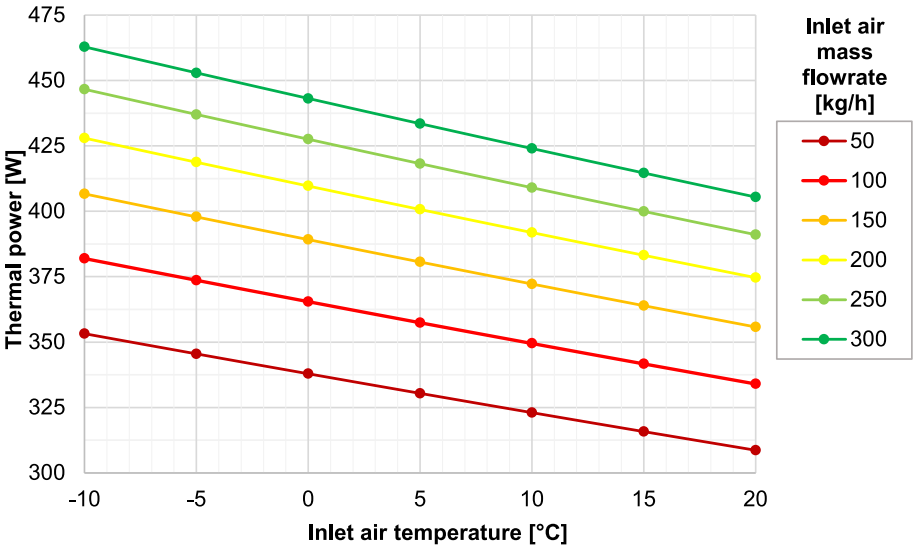


Fig. 19. The thermal power as a function of inlet air temperature and air mass flowrate.

basis during the dynamic regime of operation and deactivation of the heat source;

- the sensitivity analysis performed with the validated model reveals that the solar chimney performance is more sensitive to the variation of the inlet air temperature at higher radiation intensities than at lower radiation intensities. Precisely, the increase of air temperature between −10 and 20 °C at 1000 W/m^2 determines a decrease of thermal power of 53.4 W, while for radiation of 100 W/m^2, the decrease is 8.9 W.
- the simulations show that the effect of a higher flow rate on the thermal output is more significant at higher radiation intensities. At 1 000 W/m^2, the thermal power increases by 100.9 W when the flow rate shifts from 50 kg/h to 300 kg/h, while for 100 W/m^2 the increase is 12.5 W.

The outcomes of this study confirm the satisfactory thermal performance of the developed solar chimney and its potential to be adopted in buildings installations in order to assist heating/ventilation operation.

Further investigations are planned as some simplifications have been made in the measurements and calculations. The authors are willing to carry out seasonal field tests to determine the operating parameters under real operating conditions.

Declaration of competing interest

The authors declare that they have no known competing financial interests or personal relationships that could have appeared to influence the work reported in this paper.

Data availability

The authors are unable or have chosen not to specify which data has been used.

Acknowledgment

This work was carried out under Subvention no. 16.16.210.476 from the Faculty of Energy and Fuels, AGH University of Krakow. The research project was partly supported by the „Excellence initiative – research university" program for the AGH University of Science and Technology. The substantive support of the Cebud company and the Institute of Sustainable Energy in Krakow was obtained.

References

[1] H. Zhong, J. Wang, H. Jia, Y. Mu, S. Lv, Vector field-based support vector regression for building energy consumption prediction, Appl Energy 242 (2019) 403–414, https://doi.org/10.1016/J.APENERGY.2019.03.078.

[2] F. Filippidou, N. Nieboer, H. Visscher, Are we moving fast enough? The Energy Renovation Rate of the Dutch Non-Profit Housing Using the National Energy Labelling Database, Energy Policy 109 (2017) 488–498, https://doi.org/10.1016/J.ENPOL.2017.07.025.

[3] D.A. Krawczyk, Analysis of Energy Consumption for Heating in a Residential House in Poland, Energy Procedia 95 (2016) 216–222, https://doi.org/10.1016/J.EGYPRO.2016.09.053.

[4] F.L. Rashid, M.A. Eleiwi, H.I. Mohammed, A. Ameen, S. Ahmad, A Review of Using Solar Energy for Cooling Systems: Applications, Challenges, and Effects, Energies 2023, Vol. 16, Page 8075 16 (2023) 8075. https://doi.org/10.3390/EN16248075.

[5] F. Garde, J. Ayoub, L. Aelenei, D. Aelenei, A. Scognamiglio, Solution sets for net zero energy buildings: feedback from 30 buildings worldwide, John Wiley & Sons, Hoboken, NJ, USA, 2017 https://www.wiley.com/en-us/Solution+Sets+for+Net+Zero+Energy+Buildings%3A+Feedback+from+30+Buildings+Worldwide-p-9783433030721 (accessed November 8, 2022.

[6] K. Sornek, K. Papis-Frączek, Development and Tests of the Solar Air Heater with Thermal Energy Storage, Energies 2022, Vol. 15, Page 6583 15 (2022) 6583. https://doi.org/10.3390/EN15186583.

[7] K. Sornek, K. Papis-Fr, F. Calise, F. Liberato Cappiello, M. Vicidomini, A Review of Experimental and Numerical Analyses of Solar Thermal Walls, Energies 2023, Vol. 16, Page 3102 16 (2023) 3102. https://doi.org/10.3390/EN16073102.

[8] K.J. Khatod, V.P. Katekar, S.S. Deshmukh, An evaluation for the optimal sensible heat storage material for maximizing solar still productivity: A state-of-the-art review, J Energy Storage 50 (2022) 104622, https://doi.org/10.1016/J.EST.2022.104622.

[9] Q. Wang, G. Zhang, Q. Wu, W. Li, L. Shi, A combined wall and roof solar chimney in one building, Energy 240 (2022) 122480, https://doi.org/10.1016/J.ENERGY.2021.122480.

[10] M. Dabaieh, A. Elbably, Ventilated Trombe wall as a passive solar heating and cooling retrofitting approach; a low-tech design for off-grid settlements in semi-arid climates, Solar Energy 122 (2015) 820–833, https://doi.org/10.1016/J.SOLENER.2015.10.005.

[11] N. Monghasemi, A. Vadiee, A review of solar chimney integrated systems for space heating and cooling application, Renewable and Sustainable Energy Reviews 81 (2018) 2714–2730, https://doi.org/10.1016/J.RSER.2017.06.078.

[12] O.K. Ahmed, O.K. Ahmed, Recent Advances in Photovoltaic-Trombe Wall System: A Review, Renewable Energy - Technologies and Applications (2020), https://doi.org/10.5772/INTECHOPEN.90618.

[13] Q. Xiong, H.M. Alshehri, R. Monfaredi, T. Tayebi, F. Majdoub, A. Hajjar, M. Delpisheh, M. Izadi, Application of phase change material in improving trombe wall efficiency: An up-to-date and comprehensive overview, Energy Build 258 (2022) 111824, https://doi.org/10.1016/J.ENBUILD.2021.111824.

[14] M. Tenpierik, Y. Wattez, M. Turrin, T. Cosmatu, S. Tsafou, Temperature Control in (Translucent) Phase Change Materials Applied in Facades: A Numerical Study, Energies 2019, Vol. 12, Page 3286 12 (2019) 3286. https://doi.org/10.3390/EN12173286.

[15] H.M. Maghrabie, M.A. Abdelkareem, K. Elsaid, E.T. Sayed, A. Radwan, H. Rezk, T. Wilberforce, A.G. Abo-Khalil, A.G. Olabi, A review of solar chimney for natural ventilation of residential and non-residential buildings, Sustainable Energy Technologies and Assessments 52 (2022) 102082, https://doi.org/10.1016/J.SETA.2022.102082.

[16] L. Shi, G. Zhang, W. Yang, D. Huang, X. Cheng, S. Setunge, Determining the influencing factors on the performance of solar chimney in buildings, Renewable and Sustainable Energy Reviews 88 (2018) 223–238, https://doi.org/10.1016/J.RSER.2018.02.033.
[17] M.M. Villar-Ramos, E.V. Macias-Melo, K.M. Aguilar-Castro, I. Hernández-Pérez, J. Arce, J. Serrano-Arellano, H.P. Díaz-Hernández, L.M. López-Manrique, Parametric analysis of the thermal behavior of a single-channel solar chimney, Solar Energy 209 (2020) 602–617, https://doi.org/10.1016/J.SOLENER.2020.08.072.
[18] H. Zhang, Y. Tao, K. Nguyen, F. Han, J. Li, L. Shi, A wall solar chimney to ventilate multi-zone buildings, Sustainable Energy Technologies and Assessments 47 (2021) 101381, https://doi.org/10.1016/J.SETA.2021.101381.
[19] X. Zha, J. Zhang, M. Qin, Experimental and Numerical Studies of Solar Chimney for Ventilation in Low Energy Buildings, Procedia Eng 205 (2017) 1612–1619, https://doi.org/10.1016/J.PROENG.2017.10.294.
[20] S. Sivalakshmi, M. Raja, R. Mahudeswaran, G. Gowtham, Thermal performance of wall solar chimney integrated with a room under warm and humid conditions, Mater Today Proc 43 (2021) 1892–1895, https://doi.org/10.1016/J.MATPR.2020.10.833.
[21] A.M. Shaari, K. Abdullah, M.F. Mohideen Batcha, H. Salleh, M. Wae-Hayee, Effect of Converging Duct on Solar Chimney, CFD Letters 12 (2020) 89–97.
[22] Y.Q. Nguyen, J.C. Wells, A numerical study on induced flowrate and thermal efficiency of a solar chimney with horizontal absorber surface for ventilation of buildings, Journal of Building Engineering 28 (2020) 101050, https://doi.org/10.1016/J.JOBE.2019.101050.
[23] H. Shi, W. Chen, Thermal analysis on porous evaporation composite wall integrated with solar chimney, Appl Therm Eng 251 (2024) 123603, https://doi.org/10.1016/J.APPLTHERMALENG.2024.123603.
[24] S.K. Nateghi, M.H. Jahangir, Performance evaluation of solar chimneys in providing the thermal comfort range of the building using phase change materials, Cleaner Materials 5 (2022) 100120, https://doi.org/10.1016/J.CLEMA.2022.100120.
[25] L. Shi, Q. Wu, G. Zhang, Q. Wang, A theoretical and numerical analysis of solar chimney in multi-storey atrium building, Sustainable Energy Technologies and Assessments 65 (2024) 103797, https://doi.org/10.1016/J.SETA.2024.103797.
[26] T. Long, N. Zhao, W. Li, S. Wei, Y. Li, J. Lu, S. Huang, Z. Qiao, Numerical simulation of diurnal and annual performance of coupled solar chimney with earth-to-air heat exchanger system, Appl Therm Eng 214 (2022) 118851, https://doi.org/10.1016/J.APPLTHERMALENG.2022.118851.
[27] L. Shi, X. Cheng, L. Zhang, Z. Li, G. Zhang, D. Huang, J. Tu, Interaction effect of room opening and air inlet on solar chimney performance, Appl Therm Eng 159 (2019) 113877, https://doi.org/10.1016/J.APPLTHERMALENG.2019.113877.
[28] V. Lohmann, P. Santos, Trombe Wall Thermal Behavior and Energy Efficiency of a Light Steel Frame Compartment: Experimental and Numerical Assessments, Energies 2020, Vol. 13, Page 2744 13 (2020) 2744. https://doi.org/10.3390/EN13112744.
[29] Y. Zhu, T. Zhang, Q. Ma, H. Fukuda, Thermal Performance and Optimizing of Composite Trombe Wall with Temperature-Controlled DC Fan in Winter, Sustainability 2022, Vol. 14, Page 3080 14 (2022) 3080. https://doi.org/10.3390/SU14053080.
[30] M. Owczarek, Thermal Fluxes and Solar Energy Storage in a Massive Brick Wall in Natural Conditions, Energies 2021, Vol. 14, Page 8093 14 (2021) 8093. https://doi.org/10.3390/EN14238093.
[31] P. Miąsik, J. Krasoń, Thermal Efficiency of Trombe Wall in the South Facade of a Frame Building, Energies 2021, Vol. 14, Page 580 14 (2021) 580. https://doi.org/10.3390/EN14030580.
[32] S.A. Kostikov, J. Yiqiang, N.V. Grinkrug, Employment of a Trombe wall in Modern Heating Systems, IOP Conf Ser Mater Sci Eng 753 (2020) 022017, https://doi.org/10.1088/1757-899X/753/2/022017.
[33] D. Fidaros, C. Baxevanou, M. Markousi, A. Tsangrassoulis, Assessment of Various Trombe Wall Geometries with CFD Study, Sustainability 2022, Vol. 14, Page 4877 14 (2022) 4877. https://doi.org/10.3390/SU14094877.
[34] L. Licholai, A. Starakiewicz, J. Krasoń, P. Miąsik, The Influence of Glazing on the Functioning of a Trombe Wall Containing a Phase Change Material, Energies 2021, Vol. 14, Page 5243 14 (2021) 5243. https://doi.org/10.3390/EN14175243.
[35] S. Liu, Y. Li, An experimental study on the thermal performance of a solar chimney without and with PCM, Renew, Energy 81 (2015) 338–346, https://doi.org/10.1016/J.RENENE.2015.03.054.
[36] S. Huang, W. Li, J. Lu, Y. Li, Z. Wang, S. Zhu, Experimental study on thermal performances of a solar chimney with and without PCM under different system inclination angles, Energy 290 (2024) 130154, https://doi.org/10.1016/J.ENERGY.2023.130154.
[37] A. Mabrouki, Y. Bennani Karim, H. Ouadghiri Hassani, Y. Jamali, A. Khaldoun, A study of a passive heating design employing a Trombe wall with PCM: A numerical investigation of the semi-oceanic climate in Morocco, Mater Today Proc (2022). https://doi.org/10.1016/J.MATPR.2022.08.410.
[38] E. Leang, P. Tittelein, L. Zalewski, S. Lassue, Impact of a Composite Trombe Wall Incorporating Phase Change Materials on the Thermal Behavior of an Individual House with Low Energy Consumption, Energies 2020, Vol. 13, Page 4872 13 (2020) 4872. https://doi.org/10.3390/EN13184872.
[39] A.U. Rehman, S.R. Sheikh, Z. Kausar, S.J. Mccormack, Z.; Kausar, S.J. Mccormack, G. Zsembinszki, Numerical Simulation of a Novel Dual Layered Phase Change Material Brick Wall for Human Comfort in Hot and Cold Climatic Conditions, Energies 2021, Vol. 14, Page 4032 14 (2021) 4032. https://doi.org/10.3390/EN14134032.
[40] D. Liang, M. Ibrahim, T. Saeed, A.M. El-Refaey, Z. Li, M.A. Fagiry, Simulation of a Trombe wall with a number of semicircular fins placed on the absorber plate for heating a room in the presence of nano-PCM, Journal of Building Engineering 50 (2022) 104173, https://doi.org/10.1016/J.JOBE.2022.104173.
[41] M.E. Tiji, W.K. Al-Azzawi, H.I. Mohammed, A. Dulaimi, F.L. Rashid, J.M. Mahdi, H. S. Majdi, P. Talebizadehsardari, H.M. Ali, Thermal Management of the Melting Process in a Latent Heat Triplex Tube Storage System Using Different Configurations of Frustum Tubes, J Nanomater 2022 (2022) 7398110, https://doi.org/10.1155/2022/7398110.
[42] H.I. Mohammed, Discharge improvement of a phase change material-air-based thermal energy storage unit for space heating applications using metal foams in the air sides, Heat Transfer 51 (2022) 3830–3852, https://doi.org/10.1002/HTJ.22479.
[43] M. Tao, L. Zhenpeng, Z. Jiaxin, Photovoltaic panel integrated with phase change materials (PV-PCM): technology overview and materials selection, Renewable and Sustainable Energy Reviews 116 (2019) 109406, https://doi.org/10.1016/J.RSER.2019.109406.
[44] A. Karthick, K. Kalidasa Murugavel, A. Ghosh, K. Sudhakar, P. Ramanan, Investigation of a binary eutectic mixture of phase change material for building integrated photovoltaic (BIPV), in: System, Solar Energy Materials and Solar Cells 207, 2020, p. 110360, https://doi.org/10.1016/J.SOLMAT.2019.110360.
[45] F.L. Rashid, A. Rahbari, R.K. Ibrahem, P. Talebizadehsardari, A. Basem, A. Kaood, H.I. Mohammed, M.H. Abbas, M.A. Al-Obaidi, Review of solidification and melting performance of phase change materials in the presence of magnetic field, rotation, tilt angle, and vibration, J Energy Storage 67 (2023) 107501, https://doi.org/10.1016/J.EST.2023.107501.
[46] K. Sornek, M. Filipowicz, K. Rzepka, Study of clean combustion of wood in a stove-fireplace with accumulation, Journal of the Energy Institute 90 (2017), https://doi.org/10.1016/j.joei.2016.05.001.
[47] K. Sornek, M. Filipowicz, K. Rzepka, The development of a thermoelectric power generator dedicated to stove-fireplaces with heat accumulation systems, Energy Convers Manag 125 (2016), https://doi.org/10.1016/j.enconman.2016.05.091.
[48] S.A. Klein, et al., Solar Energy Laboratory, University of Wisconsin, Madison, TRNSYS. A transient system simulation program, 2006.